RSC Advances

PAPER

View Article Online
View Journal | View Issue

Cite this: *RSC Adv.*, 2017, **7**, 52801

Theoretical study of the Cl-initiated atmospheric oxidation of methyl isopropenyl ketone†

Yan Zhao,[a] Shengli Zou,[b] Yuan-Ye Jiang[c] and Siwei Bi*[c]

The Cl-initiated atmospheric oxidation mechanism of methyl isopropenyl ketone (MIK) has been investigated at the CCSD(T)/6-311++G(d,p)//MP2/6-311G(d,p) level of theory. Two reaction types initiated from Cl-addition and H-abstraction, respectively, and the key intermediates involved, IM1, IM2 (obtained from Cl-addition) and IM6 (obtained from H-abstraction), are presented and discussed. The calculated results supported the experimental results that Cl addition dominates the initial reactions of MIK with Cl atoms, and the most energetically favorable pathway is the Cl addition to the terminal carbon of C=C bond. Among the four proposed H abstraction processes, our study clearly indicated that the H-abstraction by Cl only takes place at the methyl linking to the internal alkenfinic carbon rather than the one at the methyl linking to the carbonyl carbon, which resolves the uncertainty of H-abstraction encountered in experiment. In addition, the isomerization processes involved in the Cl addition mechanism (1,4-H shift isomerization of IMa3 and 1,5-H shift isomerization of IMb3) were proposed in this work and found to be feasible. Both the major products experimentally detected and those derived from our theoretical study have been identified. The rate constants of the initial reactions over the atmospheric temperature range of 180–380 K have been determined using the MESMER program on the basis of Rice–Ramsperger–Kassel–Marcus (RRKM) theory. One the basis of the kinetic data we obtained, the Arrhenius formula of the total rate constant has been deduced: $k_{tot} = (5.31 \times 10^{-11})\exp(-335.24/T)$ cm^3 per molecule per s. The atmospheric lifetime of MIK in the presence of Cl atoms is calculated to be about 170.01 h.

Received 25th August 2017
Accepted 2nd November 2017

DOI: 10.1039/c7ra09445k

rsc.li/rsc-advances

1. Introduction

Methyl isopropenyl ketone (MIK, $H_2C{=}C(CH_3)C(O)CH_3$) is an important α,β-unsaturated ketone and has been observed from anthropogenic sources (plants, solvent use, biomass burning, fossil fuel combustion, *etc.*).[1–4] In addition, MIK has been found to be an intermediate product in synthesis and in the catalysis industry.[5] It is reported that MIK can be widely used in the polymer manufacturing industry.[6] MIK is highly toxic, and can cause eye, nose, throat, and skin irritation. Exposure to excessive vapor concentration may cause severe damage to eyes, possibly leading to some permanent impairment of vision.[7] Due to its high vapor pressure (42 mmHg, at 298 K), MIK is mainly released into the environment as a vapor under general atmospheric conditions.[8] The atmospheric concentration of MIK is increasing year by year because of the increasing industrial dosage. It will undergo chemical transformation or degradation to produce some secondary pollutants that have a potential contribution to air quality on regional and global scales.[9] To assess the atmospheric behavior of pollutants, it is crucial to understand their atmospheric reactions.

Once in the atmosphere, MIK can undergo photolysis and gas-phase reactions initiated by oxidants like OH and NO_3 radicals, O_3 molecules or Cl atoms, which leads to its removal from the atmosphere. Photodissociation appears to be insignificant for α,β-unsaturated ketones, since they do not absorb radiation at actinic wavelengths.[10] Although the reaction of MIK with OH radicals is generally considered to be the predominant degradation pathway among these various species, the reaction of MIK with Cl atoms also represents a significant loss process in some special regions, such as coastal regions, the marine boundary layer and some polluted mid-continental regions with high chlorine emissions.[11–13] According to Chang's report, the average concentration of Cl atoms is estimated to be as high as 3×10^5 molecules per cm^3 or more in the marine boundary layer.[14] In addition, the Cl atoms reactions with organic compounds have been reported to be much faster than OH-participated reactions.[15] Thus, it is necessary to study the Cl-initiated oxidation of MIK in order to assess its potential impact to the atmosphere.

[a]*School of Life Sciences, Qufu Normal University, Qufu, 273165, P. R. China*
[b]*Department of Chemistry, University of Central Florida, 4111 Libra Drive, Orlando, Florida 32816-2366, USA*
[c]*School of Chemistry and Chemical Engineering, Qufu Normal University, Qufu 273165, P. R. China. E-mail: siweibi@126.com*

† Electronic supplementary information (ESI) available. See DOI: 10.1039/c7ra09445k

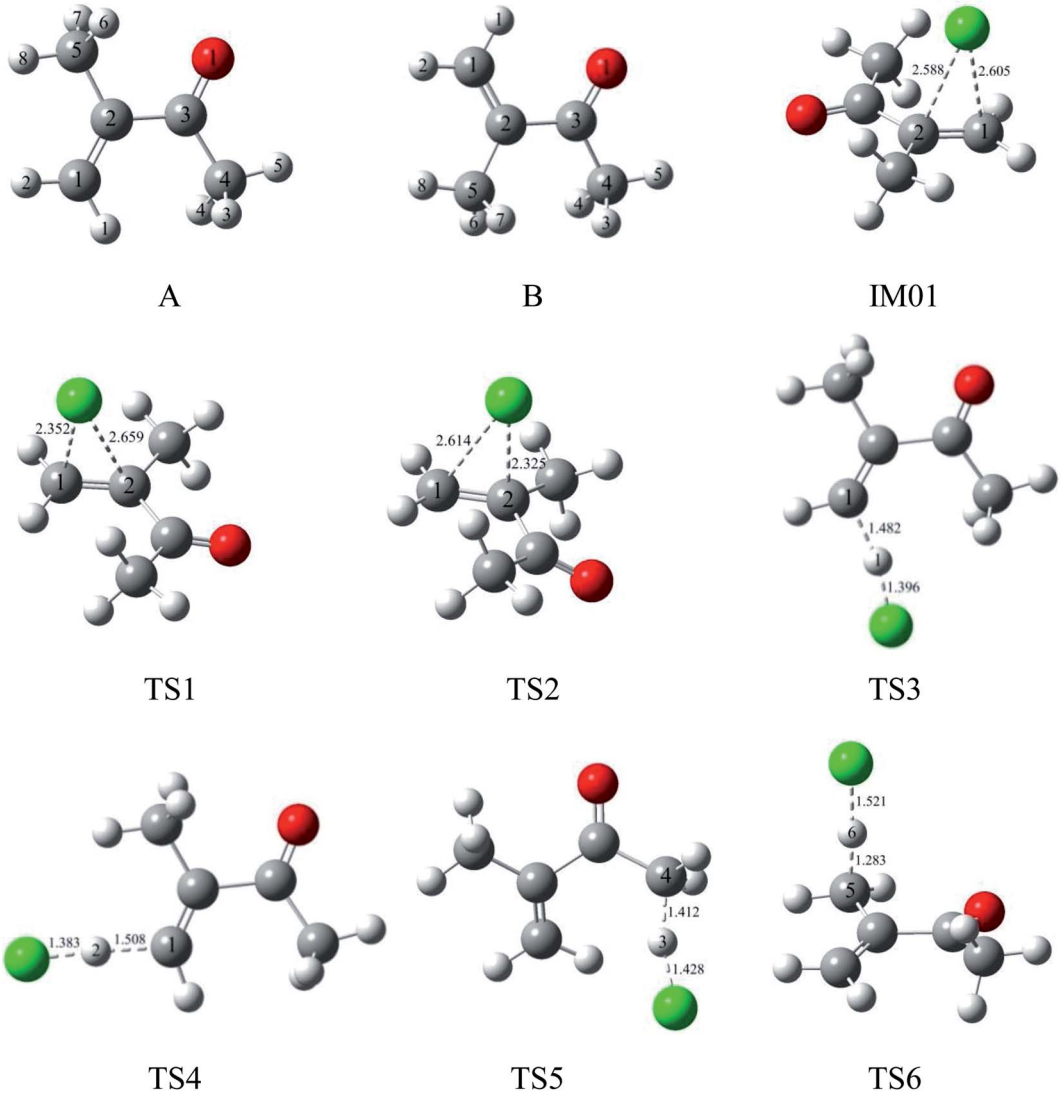

Fig. 1 Optimized geometries for reactants, pre-complexes, and transition states in the initial reaction of MIK with Cl atoms at the MP2/6-311G(d,p) level. Bond lengths are given in Å.

To date, only two experimental studies have been conducted concerning the gas-phase oxidation of MIK. In 2005, Canosa-Mas *et al.* performed the kinetic study on NO_3-initiated reactions of a series of α,β-unsaturated ketones using the relative-rate technique at 298 ± 2 K and 760 ± 5 Torr. In their study, the rate constant for reaction of NO_3 with MIK was given as (8.27 ± 6.44) × 10^{-15} cm^3 per molecule per s.[16] In 2015, Wang *et al.* determined the rate constants and products for the gas-phase reactions of atomic Cl and O_3 with MIK in a 100 L Teflon chamber at the conditions of 293 ± 1 K and atmospheric pressure. The obtained rate constants were (2.38 ± 0.26) × 10^{-10} and (1.18 ± 0.21) × 10^{-17} cm^3 per molecule per s, respectively. Several reaction products were identified by means of proton-transfer-reaction mass spectrometry (PTR-MS).[17] Furthermore, possible reaction mechanism for the reaction of Cl atoms with MIK was tentatively proposed based on the observed products.[17] However, several important questions are not solved in the experimental work. Firstly, the H-abstraction occurring at C_4 or C_5 is uncertain (see Fig. 1A). Secondly, the alkoxy radical isomerization processes should be probed although not considered experimentally. Thirdly, the rate coefficients were not studied over the general range of temperatures (for instance, 180–380 K) in the troposphere. Quantum calculations have been proven to be especially suitable for calculating the geometrical structures of the reactants, intermediates, transition states and products involved in the detailed reaction mechanism, establishing the feasibility of a reaction pathway, and investigating the kinetic properties of reactions. In this paper, the comprehensive kinetic and mechanistic studies concerning the Cl-initiated atmospheric reaction of MIK are carried out using theoretical methods.

2. Computational methods

All the quantum chemical calculations reported in this paper are performed using the Gaussian 09 program operated in

a Linux system.[18] The geometric parameters of the stationary points including reactants (R), intermediates (IM), transition states (TS), and products (P) are fully optimized using the second-order Møller–Plesset perturbation theory (MP2) with standard 6-311G(d,p) basis set.[19–21] This MP2 method has been used successfully in previous studies on the similar reaction systems.[22–25] The zero point vibrational energy (ZPE), the Gibbs free energy, the enthalpy, the entropy and the harmonic vibrational frequencies of various species are obtained at the MP2/6-311G(d,p) level (see Tables S1 and S2†). Each transition state is verified to connect the designated reactants and products by performing an intrinsic reaction coordinate (IRC)[26,27] analysis. To obtain more accurate energetic data, the single-point energy calculations are carried out at the coupled-cluster singles and doubles plus perturbative triples CCSD(T) method with 6-311++G(d,p) basis set.[28] Unless otherwise specified, the energies in this paper include the zero-point energy (ZPE) corrections and scaled by a scaling factor 0.95.[29] In other word, these $\Delta(E + \mathrm{ZPE})$ values at CCSD(T)/6-311++G(d,p)//MP2/6-311G(d,p) + 0.95 × ZPE level were used for the reaction mechanism analysis and kinetic calculations. Furthermore, the T1 diagnostic values have been calculated at the CCSD(T)/6-311++G(d,p) level (see Table S3†) and the values of all the species are less than 0.045,[30,31] which implies that the energy data obtained from single-determinant wave function of CCSD(T) are reasonably reliable for this reaction system.

The calculations of rate constants at several temperatures for the primary reactions are performed by employing Rice–Ramsperger–Kassel–Marcus (RRKM) theory with the open source MESMER program.[32,33] The RRKM reaction rate constants are calculated using the following equation:

$$k(E) = \frac{W(E)}{h\rho(E)} \quad (1)$$

where, $W(E)$ is the rovibrational sum of states at the transition state, $\rho(E)$ is density of states of reactants, and h is Planck's constant. The canonical rate constant $k(T)$ is calculated using the following equation:

$$k(T) = \frac{1}{Q(T)} \int k(E)\rho(E)\exp(-\beta E)\mathrm{d}E \quad (2)$$

where, $Q(T)$ is the reactant partition function and $\beta = 1/k_{\mathrm{B}}T$, where k_{B} is the Boltzmann's constant and T is the temperature.

3. Results and discussion

As shown in Fig. 1, two different conformers, labeled as A and B, are considered due to the internal rotation around the C_2–C_3 single bond of MIK. According to our calculation, the relative energy of conformer A is 1.95 kcal mol^{-1} lower than that of B. Therefore, the more stable conformer, A, is chosen for the following investigation.

3.1 Initial reactions of MIK with Cl atoms

For the convenience of discussion, the atomic number in MIK (conformer A) is labeled in Fig. 1. Apparently, there exist C=C and C–H bonds in the molecular structure of MIK. Thus, the initial reactions of MIK with Cl atoms can be classified as two types: Cl addition to C=C bond and H abstraction from the C–H bonds. The two types of reactions can be supported by Wang's recent experimental work.[17] Here the channels of Cl addition to the C=C double bond and H abstraction from the C–H bonds will be studied in detail. The reaction schemes embedded with the potential barriers $\Delta E^{\neq}$ and reaction heats ΔH are presented in Fig. 2.

As seen in Fig. 2, the Cl-addition reactions would proceed through two distinct reaction pathways due to the unequivalence of C_1 and C_2 positions in the double bonds of MIK. For both reaction pathways, the first step leads to the formation of the same pre-reaction complex IM01. In IM01, the distances of C_1–Cl (chlorine atom) and C_2–Cl are 2.605 and 2.588 Å, respectively. The energy of IM01 are 5.59 kcal mol^{-1} lower than the total energy of the separated reactants (MIK and Cl). Subsequently, IM01 transfers to two radical adducts (IM1 and IM2) *via* transition states TS1 and TS2 with the imaginary frequencies of 416.70i and 430.14i cm^{-1}, respectively. IRC calculations show that TS1 and TS2 do connect IM01 with IM1 and IM2, respectively. The energy barrier and exothermic heat of the two pathways are 0.31, 12.68 and 1.08, 5.24 kcal mol^{-1}, respectively. Evidently, both Cl-addition pathways are energetically favorable and can readily occur under the general atmospheric conditions.

In MIK molecule structure, the eight H atoms linked to different carbon atoms fall into six species according to their different chemical environment. Therefore, six possible processes are identified: H-abstractions of H_1, H_2, H_3, H_5, H_6 and H_8 atoms. The H-abstractions of H_3 and H_5 atoms occur through the same transition state since the C_3–C_4 bond is rotatable. Similarly, H_6 and H_8 abstraction processes proceed *via* the same transition state due to the rotation of C_2–C_5 bond. Hence, only four H abstraction pathways are considered and depicted in Fig. 2. Four transition states (TS3, TS4, TS5, and TS6) are located, and each one is identified with only one imaginary frequency. Furthermore, the validity of each transition-state structure is determined by IRC calculations. The geometrical parameters of the four transition states are presented in Fig. 1. Following H abstraction, four intermediate radicals IM3, IM4, IM5, and IM6 are generated. As given in Fig. 2, the energy barriers of the four H abstraction processes are 15.00, 13.20, 14.27 and 3.26 kcal mol^{-1}, respectively. The H abstraction in C_5–H_6 bond is exothermic by 3.22 kcal mol^{-1}, while the other three channels are endothermic by 12.97, 11.16, and 10.53 kcal mol^{-1}. The energy values mentioned above show that the H abstraction from C_5 position is both thermodynamically and kinetically favorable and is easy to occur under the general conditions. In the experimental investigation reported by Wang *et al.*,[17] it is uncertain whether the H-abstraction process occurs at C_4 or C_5 positions of MIK only according to the experimental measurement. Obviously, our theoretical calculation provides a solid conformation for the feasibility of the H abstraction from C_5 position. Thus, the combination of experiment and theoretical calculation is a wonderful method to obtain more accurate conclusions in this investigation.

Comparing the two Cl-addition pathways and the four H abstraction processes, we can know that the two addition paths

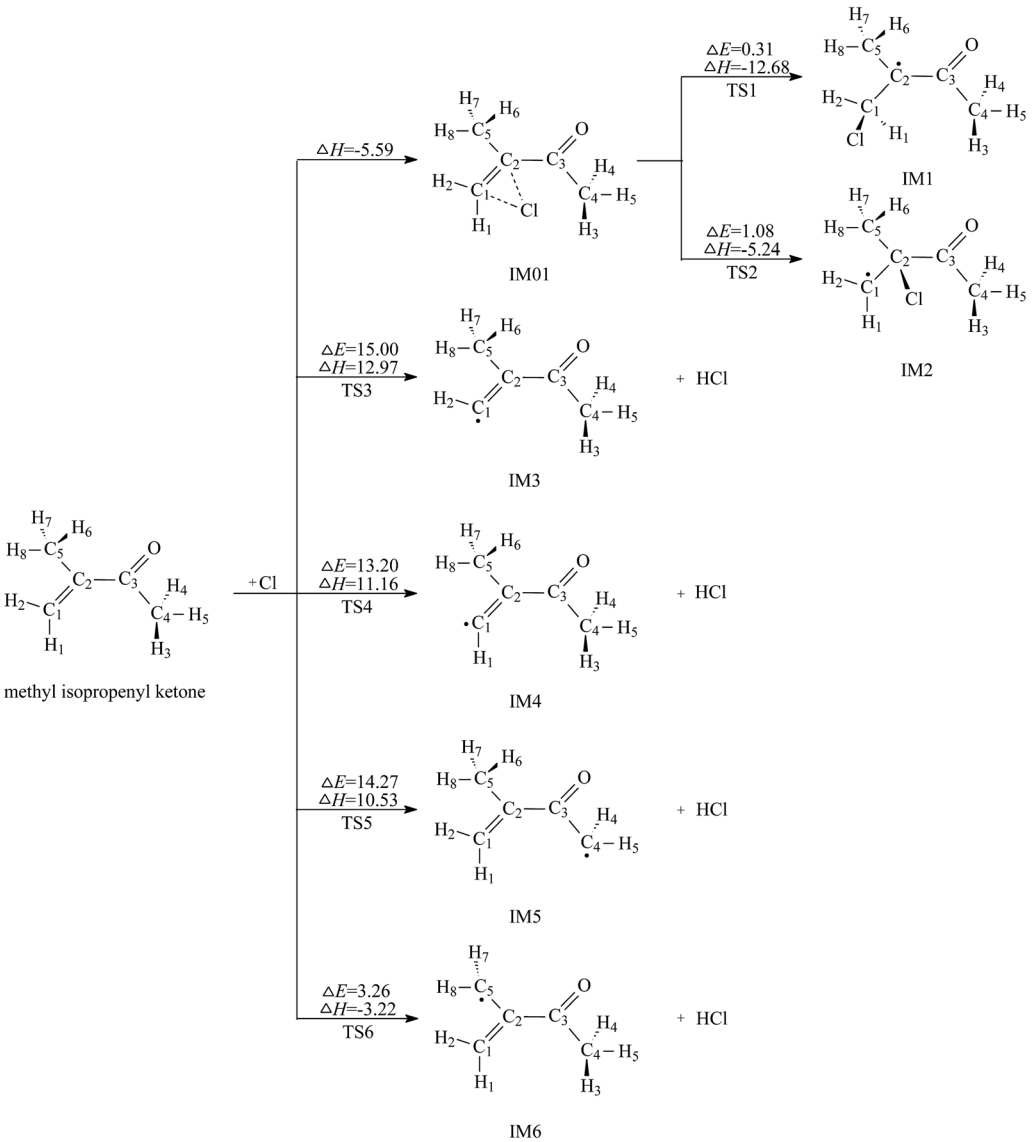

Fig. 2 Cl addition pathways and H abstraction pathways embedded with the potential barriers $\Delta E^{\neq}$ (kcal mol^{-1}) and reaction heats ΔH (kcal mol^{-1}).

are more favorable than H abstraction channels and they dominate the reaction of MIK with Cl atoms. Also, Cl addition to C_1 (terminal carbon) atom is preferred over that to C_2 because the former has a lower energy barrier and exothermicity. From the analysis of the molecular geometry, Cl addition to C_2 has the greater steric hindrance than Cl addition to C_1 (terminal carbon). This conclusion agrees well with the previous experimental study about the reaction of MIK with atomic Cl.[17] For the four H abstraction reactions, the H abstraction from C_5 position is easy to occur due to its low barrier and exothermicity, while the other three H abstraction processes can hardly to take place as they have higher potential barriers and are endothermic.

3.2 Secondary reactions

On the basis of the above discussion, it is shown that both addition and H abstraction from C_5 processes are the dominant pathways for the Cl-initiated atmospheric reaction of MIK. The corresponding products, IM1, IM2, and IM6 are important radical intermediates and their further reactions will be discussed step by step in this section.

3.2.1. Atmospheric reaction pathway of IM1. As an open-shell and highly reactive radical, IM1 can react readily with O_2 molecule to form an organic peroxy intermediate IMa1. This process is barrier-free with 37.29 kcal mol^{-1} exothermicity. In the troposphere, IMa1 will react immediately with ubiquitous NO. An energy of 23.88 kcal mol^{-1} is released to produce an excited intermediate IMa2. The geometric structures of IMa1 and IMa2 are depicted in Fig. S2.† IMa2 will undergo unimolecular decomposition which proceeds *via* the rupture of O_2–O_3 bond, leading to the oxyl radical IMa3 and NO_2. TSa1 represents the transition state for this decomposition process. The O_2–O_3 distance in TSa1 is 1.794 Å, which is 0.368 Å longer than that in IMa2. The potential barrier of this process is calculated to be 7.86 kcal mol^{-1}. IMa3 is an activated alkoxy

radical and its further reaction is inevitable in the atmosphere. Two decomposition reactions and one isomerization reaction are found and displayed in Fig. 3.

One decomposition reaction is the cleavage of C_1–C_2 bond to generate 2,3-butanedione (Pa1) and IMa4 by passing transition state TSa2 with the energy barrier value of 6.34 kcal mol^{-1}. The reaction heat of this process is −4.03 kcal mol^{-1}. Subsequently, IMa4 can be further oxidized by O_2 and nitric oxide through two barrier-free steps to produce IMa6. Both association processes are highly exothermic by 23.82 and 17.68 kcal mol^{-1}, respectively. Then, energy-rich IMa6 will promptly decompose to IMa7 and NO_2 *via* the scission of the O_1–O_2 bond. This dissociation process has a very low energy barrier of 0.93 kcal mol^{-1}. Further reaction from IMa7 is the direct H abstraction by O_2 molecule *via* the

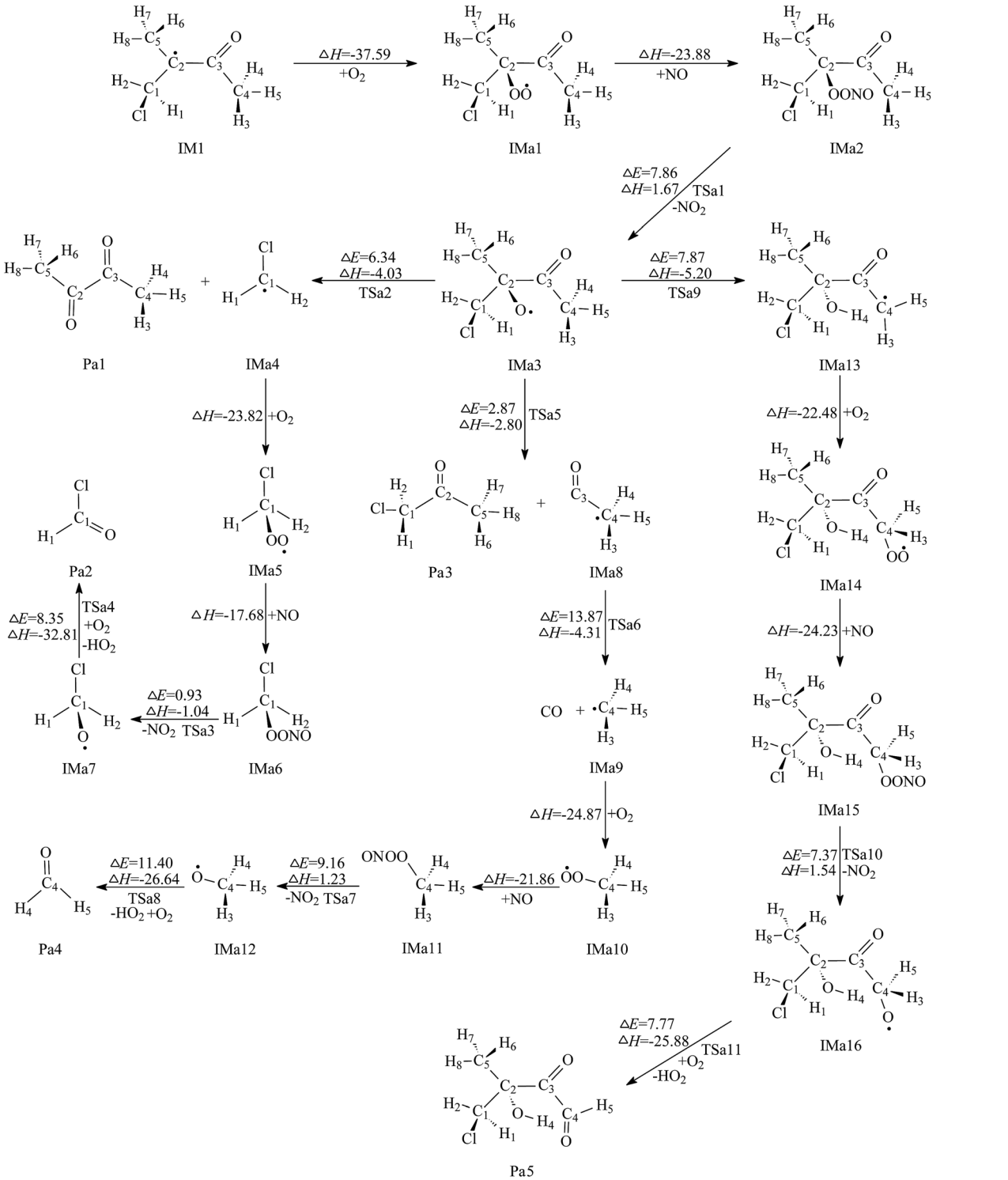

Fig. 3 Secondary reaction pathways of IM1 with the potential barriers $\Delta E^{\neq}$ (kcal mol^{-1}) and reaction heats ΔH (kcal mol^{-1}).

transition state TSa4 with the barrier height of 8.35 kcal mol^{-1}. This H abstraction process leads to the formation of formyl chloride (Pa2) and HO_2 radical with 32.81 kcal mol^{-1} heat released.

The other decomposition reaction is finished by the rupture of C_2–C_3 bond, leading to chloroacetone (Pa3) and a radical intermediate, denoted IMa8. The transition state of this process is TSa5, in which the C_2–C_3 distance is 1.860 Å (see Fig. S7†). This reaction has a low potential barrier of 2.87 kcal mol^{-1} and is exothermic by 2.80 kcal mol^{-1}, which means the decomposition reaction is energetically favorable under atmospheric condition. IMa8 has high reactivity and can easily further react *via* the fission of C_3–C_4 bond to produce CO and IMa9, with the transition state TSa6. The energy barrier and reaction heat of the process are 13.87 and −4.31 kcal mol^{-1}, respectively. The subsequent reactions of IMa9 with O_2/NO proceeds through three elementary steps to generate IMa12. Then, formaldehyde (Pa4) and HO_2 are produced from the reaction of IMa12 with O_2. It can be seen from Fig. 4 that the highest barrier of these four elementary reactions is 11.40 kcal mol^{-1}. Consequently, this formation pathway of Pa4 is energetically favorable in the atmosphere, which provides a theoretical conformation for the formation of Pa4 in experiment.

The 1,4-H shift isomerization of IMa3 to IMa13 takes place *via* a five-membered ring transition state, TSa9, with a potential barrier of 7.87 kcal mol^{-1}. The C_4–H_4 and H_4–O_2 distances in TSa9 are 1.235 and 1.295 Å, respectively. Also, the intrinsic reaction coordinate calculation verifies the synchronism of the breakage of C_4–H_4 bond and the generation of O_2–H_4 bond. The geometric structure of TSa9 is presented in Fig. S3.† Further reaction of IMa13 that results in the product of 4-chloro-3-hydroxy-3-methyl-2-oxobutanal (Pa5) involves four elementary processes: two free-barrier processes with high exothermicity and two elementary processes with low energy barriers. Accordingly, these elementary steps are both thermodynamically and kinetically favorable under atmospheric conditions. The product of Pa5 should be present in photochemical smog. Unfortunately, Pa5 was not detected in the experimental study by Wang *et al.*[17] Further experimental observation would be anticipated to confirm the formation of Pa5.

Comparing three further reactions of intermediate IMa3, we can find that the decomposition by the cleavage of C_2–C_3 bond is the most favorable pathway. Pa3 and Pa4 are the dominant products. The 1,4-H shift isomerization pathway is favorable in thermodynamics and kinetics.

3.2.2. Atmospheric reaction pathway of IM2. As depicted in Fig. 4, IM2 firstly reacts with O_2 and NO in turn to form the peroxy radical IMb2. 26.23 and 23.63 kcal mol^{-1} are the corresponding exothermic energies of the two barrierless processes. Then, energy-rich IMb2 breaks down to IMb3 and NO_2 is removed *via* TSb1, respectively with the energy barrier of 9.14 kcal mol^{-1} and endothermic heat of 1.42 kcal mol^{-1}. There are four possible reaction pathways for further reaction of the oxyl radical IMb3.

The first one is the reaction of IMb3 with O_2 molecule. In this process, H_2 atom linked to C_1 is directly abstracted by O_2 to form 2-chloro-2-methyl-3-oxobutanal (Pb1) and HO_2. TSb2 is the transition state in which the distances of C_1–H_2 and O_4–H_2 are 1.226 and 1.351 Å, respectively. Calculations indicate that this process has a low potential barrier of 3.79 kcal mol^{-1} and is strongly exothermic of 30.09 kcal mol^{-1}, which suggests that this O_2 direct abstraction can occur readily. The product of Pb1 was detected in the reaction chamber of the Cl-initiated atmospheric reaction of MIK.[17]

The second channel is unimolecular decomposition that is initiated from the C_1–C_2 bond breakage through the transition state TSb3. The formation of Pa4 and IMb4 is an exothermic process by releasing 2.76 kcal mol^{-1} heat quantities, with the energy barrier of 10.30 kcal mol^{-1}. The intermediate IMb4 then combines with O_2 and NO sequentially, forming IMb6. Both free-barrier processes are exothermic by 19.54 and 23.52 kcal mol^{-1}. Then IMb6 will be changed to IMb7 by releasing NO_2. This process should overcome 7.12 kcal mol^{-1} energies and absorb 0.66 kcal mol^{-1} heat quantities. For IMb7, two reaction channels are taken into account. The first one is the decomposition of IMb7 *via* C_2–C_3 bond scission to generate acetyl chloride (Pb2) and IMa8. The barrier height is very low, only 2.80 kcal mol^{-1}. This process is exothermic by 6.45 kcal mol^{-1}. The second channel proceeds through the C_2–C_5 bond rupture to produce 2-oxopropanoyl chloride (Pb3) and IMa9. The energy barrier and the exothermic heat of this process is calculated to be 6.87 and 6.84 kcal mol^{-1}, respectively. Thus, the decomposition pathways of IMb7 to Pb2 or Pb3 are energetically favorable. Comparing the energy barriers of the two decomposition channels, the first decomposition is more favorable than the second one, which is revealed for the first time.

The third channel of IMb3, called 1,5-H shift isomerization, occurs *via* a six-membered ring transition state, TSb7, to yield IMb8. In the structure of TSb7, the breaking C_4–H_4 bond is elongated by 12.42% with respect to the equilibrium value of 1.095 Å in IMb3, while the forming H_4–O_2 bond is shortened by 30.83% with respect to the equilibrium value of 0.960 Å in IMb8. The structure of TSb7 is illustrated in Fig. S3.† The energy barrier and the exothermic heat of this process are 10.05 and 10.54 kcal mol^{-1}, respectively. The subsequent reaction of resulting radical intermediate IMb8 can generate 3-chloro-4-hydroxy-3-methyl-2-oxobutanal (Pb4) *via* the different mechanisms which include O_2 addition, NO addition, breakage of O–ONO bond and H abstraction by O_2. The calculated profiles of the potential energy surface show that these elementary steps are easy to occur due to lower potential barriers and strong exothermicity. This indicates that the product Pb4 should be a secondary pollutant present in the experiment chamber. Unluckily, this whole isomerization pathway form IMb3 to Pb4 was not considered in previous experimental study.[17] Hence, this is the first time to report the feasible isomerization pathway of IMb3 and its conformation needs further more experimental investigations. The fourth channel of IMb3 takes place *via* H_7 migration to form IMb12. A five-membered ring transition state, TSb10, is identified as being associated with this 1,4-H shift isomerization process. The distances for the breaking C_5–H_7 and the forming H_7–O_2 are 1.248 and 1.297 Å, respectively. This isomerization process overcomes a high potential barrier of 17.47 kcal mol^{-1}, and releases an energy of 6.98 kcal mol^{-1} to the surroundings. It can be inferred that this isomerization

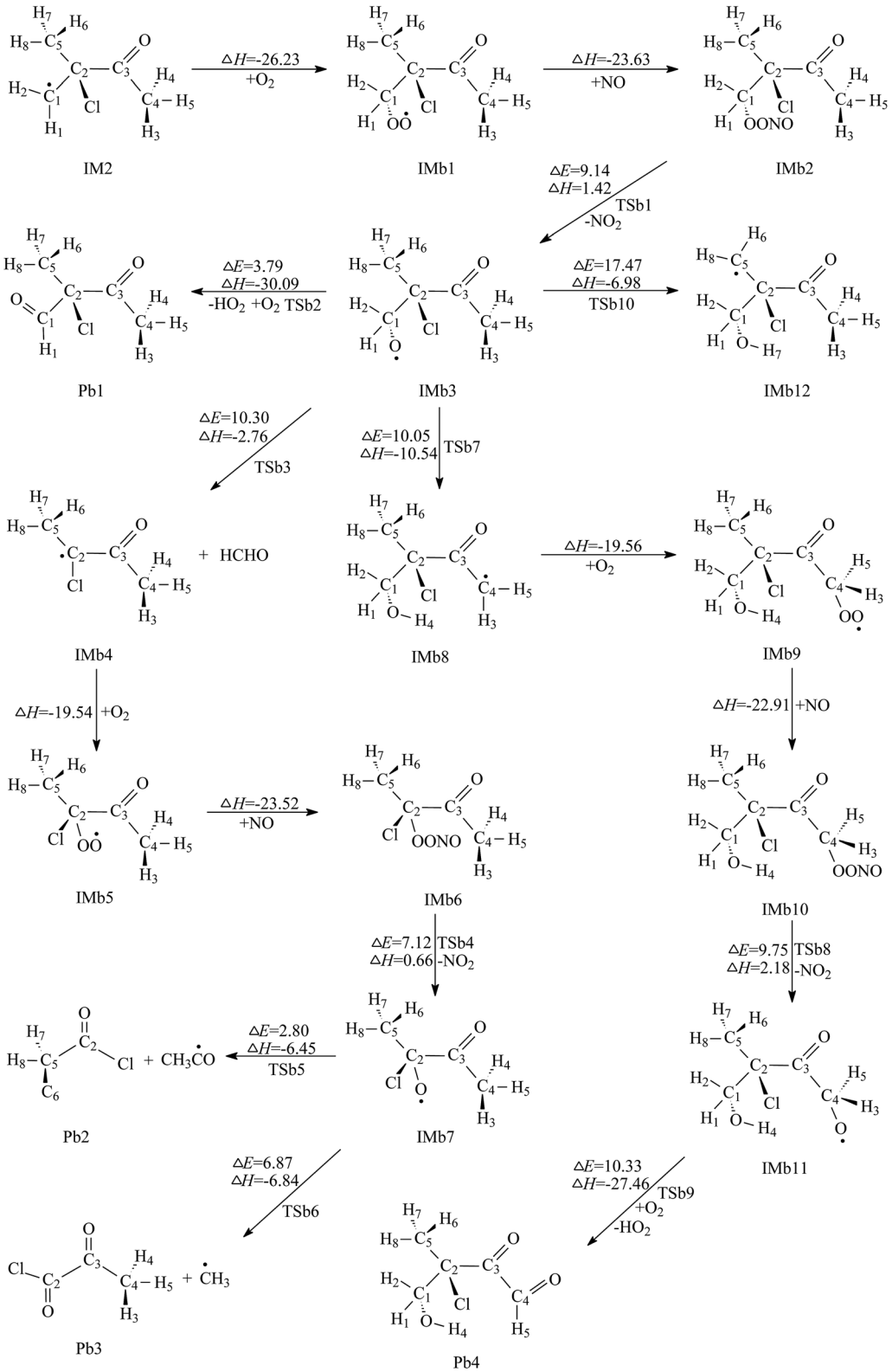

Fig. 4 Secondary reaction pathways of IM2 with the potential barriers $\Delta E^{\neq}$ (kcal mol^{-1}) and reaction heats ΔH (kcal mol^{-1}).

reaction is not expected to be important as it has a much higher energy barrier than the above three channels. Consequently, further reaction of IMb10 can be ignored.

Comparison of the calculated results reveals that the first channel (O_2 direct abstraction reaction) is preferred over the other three ones due to the lowest energy barrier. Both the

second and the third channels are competitive. Pb1 and Pb2 are the dominant products for further reaction of IMb3.

3.2.3. Atmospheric reaction pathway of IM6. IM6 is the primary intermediate produced from the hydrogen abstraction pathways of MIK by atomic Cl. Fig. 5 exhibits the possible reaction routes from IM6. Similar to IM1 and IM2, IM6 can also react with O_2/NO through three elementary steps to form NO_2 and an alkoxy radical, IMc3. The geometric parameters of IMc3 are depicted in Fig. S2.† The following reaction of IMc3 will proceed *via* three different paths under the atmospheric conditions. The first path is the O_2 direct H-abstraction, which occurs *via* TS10, followed by the loss of HO_2, to produce 2-methylene-3-oxobutanal (Pc1), with a potential barrier of 7.08 kcal mol^{-1}. This process is strongly exothermic by up to 29.04 kcal mol^{-1}. Thus, Pc1 should be the product for further reaction of IM6. The second path of IMc3 is the cleavage of C_2–C_5 bond and IMc4 + HCHO are produced *via* the transition state TSc3 with a high energy barrier of 28.64 kcal mol^{-1}. Both the reaction heat and Gibbs free energy change are positive values, 22.74 and 11.65 kcal mol^{-1}, respectively, which indicates that this decomposition process is unlikely to occur spontaneously under the atmospheric conditions. The third path is the isomerization of IMc3 *via* 1,5-H shift, which leads to IMc5. A six-membered ring transition state, TSc5, is identified with a potential barrier of 15.12 kcal mol^{-1}. This process is found to be an endothermic process, with an absorption heat of 10.65 kcal mol^{-1}. Moreover, the Gibbs free energy change is 10.30 kcal mol^{-1}, which is far greater than zero. It can be inferred that this isomerization process can not take place spontaneously.

Comparison of the above calculated data reveals that the second and the third paths, *i.e.* decomposition *via* C_2–C_5 bond fission and 1,5-H shift isomerization, can be ignored, while the first path, *i.e.* O_2 abstracting reaction, will be the dominant removal pathway of IMc3. Pc1 and HO_2 are the products for further reaction of IM6.

3.3 Rate constant calculations

Based on the above thermodynamic results, the individual and overall rate constants for the primary reactions including the Cl additions and the H abstractions are calculated with the Rice–Ramsperger–Kassel–Marcus (RRKM) theory. A suitable temperature range of 180–380 K is selected to study the relationship between the temperature and rate constant. The rate constants k_1 and k_2 are for Cl addition to C_1 and C_2 atoms, while k_3 to k_6 correspond to H abstraction from C_1–H_1, C_1–H_2, C_4–H_3, and C_5–H_6, respectively. The overall rate constant of OH-addition channels and H-abstraction reactions are denoted as k_{add}, and k_{abs}, respectively. The total rate constant for the reaction of MIK with Cl atoms is labeled as k_{tot}, where $k_{add} = k_1 + k_2$, $k_{abs} = k_3 + k_4 + 3k_5 + 3k_6$, then $k_{tot} = k_{add} + k_{abs}$.

The individual and overall rate constants are calculated in the temperature range of 180–380 K and they are fitted in the two-parameter Arrhenius formula $k = A\exp(-E_a/RT)$. The calculated rate constants and the Arrhenius formulas are given in Table 1. Under the pressure of 760 Torr and at 293 K, the calculated total rate constant is 1.87×10^{-10} cm^3 per molecule per s. This value matches well with available experimental value

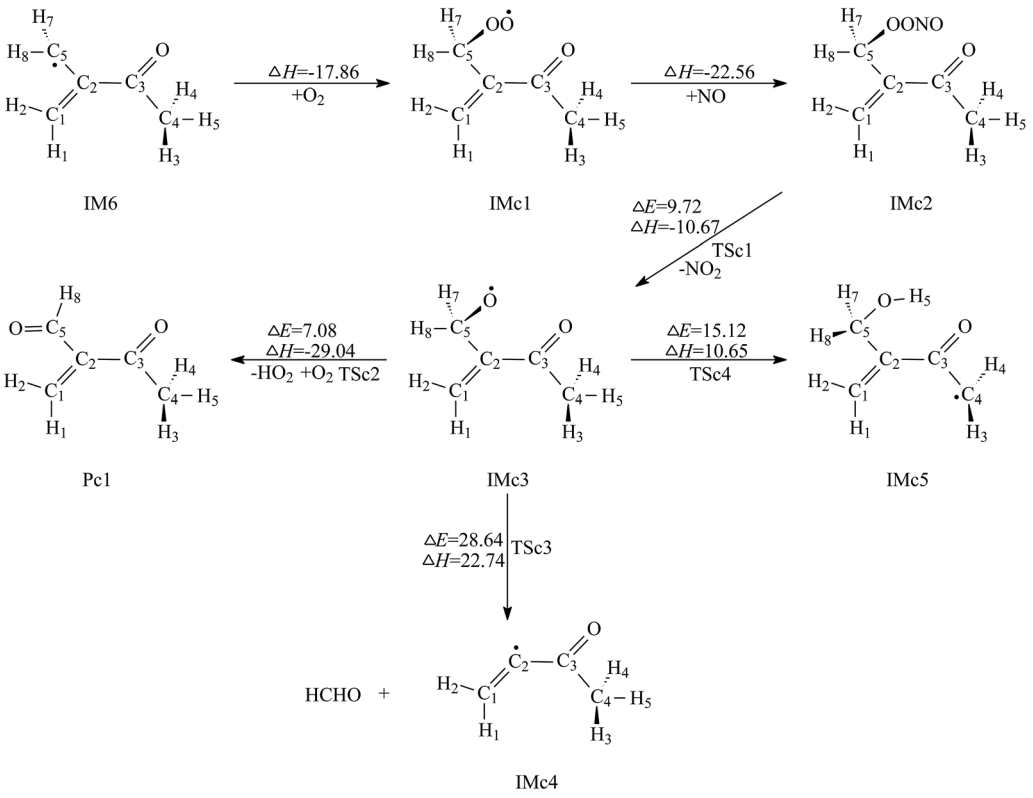

Fig. 5 Secondary reaction pathways of IM6 with the potential barriers $\Delta E^{\neq}$ (kcal mol^{-1}) and reaction heats ΔH (kcal mol^{-1}).

Table 1 Rate constants k (cm^3 per molecule per s) at 293 K and Arrhenius formulas for the reaction of MIK with Cl atoms over the temperature range of 180–380 K[a]

Reactions	Arrhenius formulas	$k_{293\ K}$
MIK + Cl → IM1	$k_1(T) = 4.18 \times 10^{-10} \exp(-373.34/T)$	1.61×10^{-10}
MIK + Cl → IM2	$k_2(T) = 8.36 \times 10^{-11} \exp(-352.33/T)$	2.19×10^{-11}
MIK + Cl → IM3 + HCl	$k_3(T) = 9.52 \times 10^{-15} \exp(-6445.13/T)$	2.61×10^{-24}
MIK + Cl → IM4 + HCl	$k_4(T) = 1.62 \times 10^{-15} \exp(-4996.08/T)$	9.19×10^{-23}
MIK + Cl → IM5 + HCl	$k_5(T) = 4.02 \times 10^{-15} \exp(-5804.12/T)$	2.05×10^{-23}
MIK + Cl → IM6 + HCl	$k_6(T) = 1.58 \times 10^{-13} \exp(-573.59/T)$	1.16×10^{-12}

[a] At 293 K, $k_{add} = 1.83 \times 10^{-10}$, $k_{abs} = 3.48 \times 10^{-12}$, $k_{tot} = 1.87 \times 10^{-10}$.

($(2.38 \pm 0.26) \times 10^{-10}$ cm^3 per molecule per s) with a maximum relative deviation of less than two times, which indicates that our calculation in this work is thought as reasonable. The ln k_{tot} *versus* $1000/T$ are depicted in Fig. 6. We can clearly see that k_{tot} shows negative temperature dependence over the studied interval. The Arrhenius equation of the total rate coefficient over the temperature of 180–380 K is fitted as $k_{tot} = (5.31 \times 10^{-11}) \exp(-335.24/T)$. It is evident from Table 1 the overall rate constant of Cl-addition reactions (1.83×10^{-10} cm^3 per molecule per s) is about two orders of magnitude higher than that of H-abstraction reactions (3.48×10^{-12} cm^3 per molecule per s) under the same conditions, which means that the Cl-addition reactions are easier to take place than the H-abstraction reactions. For the addition pathways, k_1 is nearly an order of magnitude higher than k_2, which indicates that the more favorable pathway is the Cl addition to the terminal carbon (C_1) of the C=C bond. Compared all the possible H abstraction channels, we can see that the rate constants are $k_6 > k_4 > k_5 > k_3$. Moreover, k_6 is more than ten orders of magnitude higher than k_3, k_4, and k_5. Hence, Cl abstracting the H atom from C_5 position is predominant in the abstraction reactions and the other three channels can be neglected.

The atmospheric lifetime of MIK can be calculated using the following expression:

$$\tau = \frac{1}{k[\mathrm{Cl}]}$$

Here k is the total rate constant obtained in this work and [Cl] is the atmospheric concentration of Cl which is 1.0×10^4 molecules per cm^3.[34] The calculated atmospheric lifetime of MIK determined by the concentration of Cl atoms is approximately 148.54 h, which is in good agreement with the observed value of 116.71 h. In the coastal marine boundary layer and some industrial areas, the average daytime concentration of Cl atoms is as high as 3.0×10^5 molecules per cm^3.[14] Under the circumstances, atmospheric lifetime of MIK with Cl is only 4.95 h, which suggests that Cl-initiated oxidation of MIK could compete with the corresponding hydroxylation reaction (3.86 h).[35] This implies that Cl-initiated reaction of MIK plays an important role in the marine boundary layer and some special areas.

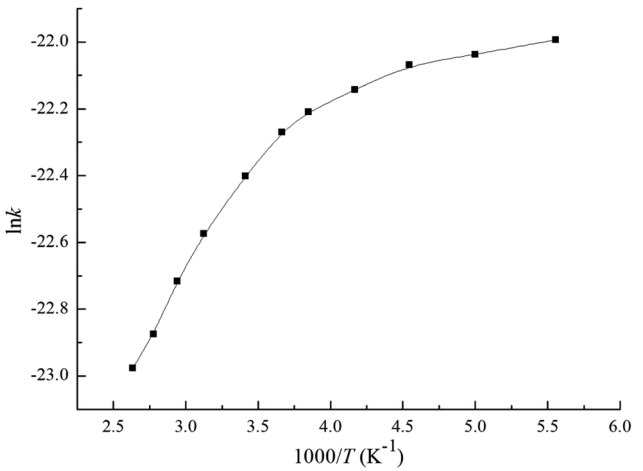

Fig. 6 Rate constants for the reaction of MIK with Cl at different temperatures and 760 Torr.

3.4 Discussion of structure impact on reaction activity

In order to evaluate the effect of structure on reaction reactivity of this series of unsaturated aldehydes and ketones, rate constants of Cl-initiated acrolein (ACR, CH_2=CHCHO), methacrolein (MACR, CH_2=C(CH_3)CHO), and methyl vinyl ketone (MVK, CH_2=CHC(O)CH_3) were calculated at 298 K and 760

Table 2 The overall rate constant of addition channels and the total rate constant for the reaction of ACR, MACR, MVK, MIK with Cl atoms at 298 K and 760 Torr

	Rate constant/10^{-10} cm^3 per molecule per s		
Compound	k_{add}	k_{tot}	k_{exp}
Acrolein	1.94	1.96	2.5 ± 0.7 (ref. 36) 2.0 ± 0.3 (ref. 37) 2.2 ± 0.3 (ref. 38)
Methacrolein	2.38	2.42	2.9 ± 0.8 (ref. 36) 3.2 ± 0.5 (ref. 39)
Methyl vinyl ketone	1.59	1.59	2.0 ± 0.5 (ref. 36) 2.0 ± 0.2 (ref. 40) 2.1 ± 0.5 (ref. 39)
Methyl isopropenyl ketone	1.82	1.86	

Torr. As displayed in Table 2, all the kinetic data are in accord with their corresponding experimental values previously reported.[36–40] Compared all the addition channels of these four compounds, we can see that the rate constants of addition channels are $k_{\text{add-MACR}} > k_{\text{add-ACR}} > k_{\text{add-MIK}} > k_{\text{add-MVK}}$. Also, the total rate constants are $k_{\text{tot-MACR}} > k_{\text{tot-ACR}} > k_{\text{tot-MIK}} > k_{\text{tot-MVK}}$. This phenomenon can be explained from the electron-donating effects of methyl group and the electron-withdrawing properties of ketone group in the concerned molecules. The inductive effect of methyl group (in methacrolein and methyl isopropenyl ketone) increases the reactivity due to the electron-donating inductive effect of the methyl group attached to the double bond. On the contrary, the adjacent ketone group (in methyl vinyl ketone and methyl isopropenyl ketone) decreases the reactivity because the oxygen has the electron-withdrawing properties.

4. Conclusions

The atmospheric oxidation reaction of MIK initiated by atomic Cl was investigated using quantum chemical methods. The conclusions are drawn as follows:

(1) Two types of reactions, Cl additions and H abstractions, involved in the initial reactions of MIK with Cl atoms, are considered based on the experimental data. Our calculations show that Cl-addition pathways are favored over H-abstraction channels and Cl addition to terminal carbon C_1 in C=C bond is the most energetically favorable pathway, which supports the experimental results. Among the four possible H abstraction processes, only the H abstraction from C_5 position is confirmed to be feasible by our study. This resolves the uncertainty of H-abstraction encountered in experiment.

(2) Four alkoxy radical isomerization processes are proposed and investigated theoretically in our work. The calculated results indicate that the two processes (1,4-H shift isomerization of IMa3 and 1,5-H shift isomerization of IMb3) can take place under atmospheric conditions. The formation of the corresponding isomerization products, 4-chloro-3-hydroxy-3-methyl-2-oxobutanal and 3-chloro-4-hydroxy-3-methyl-2-oxobutanal, needs further experimental observation. In addition, our study clearly indicated that 2-methylene-3-oxobutanal is the only product formed from the H abstractions.

(3) The calculated total rate constants match the experimental values well at the same temperature and pressure. The Arrhenius equation of the total rate coefficient over the temperature range of 180–380 K is fitted as $k_{\text{tot}} = (5.31 \times 10^{-11})\exp(-335.24/T)$. The atmospheric lifetime of MIK in the presence of Cl is estimated to be 197.01 h.

Conflicts of interest

There are no conflicts to declare.

Acknowledgements

This work was financially supported by the Shandong Province Natural Science Foundation (No. ZR2017MB050, ZR2017QB001), National Natural Science Foundation of China (No. 21473100, 21702119, 21207078) and Qufu Normal University Research Fund (No. XJ201206).

References

1 S. K. Akagi, R. J. Yokelson, I. R. Burling, S. Meinardi, I. Simpson, D. R. Blake, G. R. McMeeking, A. Sullivan, T. Lee, S. Kreidenweis, S. Urbanski, J. Reardon, D. W. T. Griffith, T. J. Johnson and D. R. Weise, *Atmos. Chem. Phys.*, 2013, **13**, 1141–1165.
2 J. D. McDonald, B. Zielinska, E. M. Fujita, J. C. Sagebiel, J. C. Chow and J. G. Watson, *Environ. Sci. Technol.*, 2000, **34**, 2080–2091.
3 D. E. Seizinger and B. Dimitriades, *J. Air Pollut. Control Assoc.*, 1972, **22**, 47–51.
4 M. Dicke, *Plant, Cell Environ.*, 2009, **32**, 654–665.
5 P. G. N. Mertens, H. Poelman, X. Ye, I. F. J. Vankelecom, P. A. Jacobs and D. E. De Vos, *Catal. Today*, 2007, **122**, 352–360.
6 U. S. Coast Guard, Department of Transportation, *CHRIS-Hazardous Chemical Data. Manual Two*, U.S. Government Printing Office, Washington, DC, Oct 1978.
7 *Industrial Hygiene and Toxicology: Volume II: Toxicology*, ed. F. Patty, Interscience Publishers, New York, 2nd edn, 1963, p. 1753.
8 *Patty's Industrial Hygiene and Toxicology: Volume 2A, 2B, 2C: Toxicology*, ed. G. D. Clayton and F. E. Clayton, John Wiley Sons, New York, 3rd edn, 1981–1982, p. 4722.
9 A. Mellouki, G. Le Bras and H. Sidebottom, *Chem. Rev.*, 2003, **103**, 5077–5096.
10 A. Mellouki, T. J. Wallington and J. Chen, *Chem. Rev.*, 2015, **115**, 3984–4014.
11 E. Galán, I. González and B. Fabbri, *Atmos. Environ.*, 2002, **36**, 5289–5298.
12 L. H. Mielke, F. Amanda and H. D. Osthoff, *Environ. Sci. Technol.*, 2011, **45**, 8889–8896.
13 J. A. Thornton, J. P. Kercher, T. P. Riedel, N. L. Wagner, C. Julie, J. S. Holloway, W. P. Dubé, G. M. Wolfe, P. K. Quinn and A. M. Middlebrook, *Nature*, 2010, **464**, 271–274.
14 C. T. Chang, T. H. Liu and F. T. Jeng, *Environ. Res.*, 2004, **94**, 67–74.
15 R. Atkinson, D. L. Baulch, R. A. Cox and J. N. Crowley, *Atmos. Chem. Phys.*, 2006, **6**, 3625–4055.
16 C. E. Canosa-Mas, M. L. Flugge, M. D. King and R. P. Wayne, *Phys. Chem. Chem. Phys.*, 2005, **7**, 643–650.
17 J. Wang, L. Zhou, W. Wang and M. Ge, *Phys. Chem. Chem. Phys.*, 2015, **17**, 12000–12012.
18 M. Frisch, G. Trucks, H. B. Schlegel, G. Scuseria, M. Robb, J. Cheeseman, G. Scalmani, V. Barone, B. Mennucci and G. Petersson, *Gaussian 09, revision A. 02*, Gaussian. Inc., Wallingford, CT, 2009, vol. 270, p. 271.
19 C. Møller and M. S. Plesset, *Phys. Rev.*, 1934, **46**, 618–622.
20 G. D. Fletcher, A. P. Rendell and P. Sherwood, *Mol. Phys.*, 1997, **91**, 431–438.
21 EMSL Basis Set Library, http://www.emsl.pnl.gov/forms/basisform.html.

22 H. Xie, F. Ma, Y. Wang, N. He, Q. Yu and J. Chen, *Environ. Sci. Technol.*, 2015, **49**, 13246–13255.
23 X. Wang, F. Bai, Y. Sun, R. Wang, X. Pan and F. Tao, *J. Phys. Chem. A*, 2017, **121**, 226–237.
24 W. Zhang and D. Zhang, *Mol. Phys.*, 2012, **110**, 2901–2917.
25 P. Biswas, *J. Theor. Comput. Chem.*, 2015, **14**, 1550010.
26 C. Gonzalez and H. B. Schlegel, *J. Chem. Phys.*, 1989, **90**, 2154–2161.
27 C. Gonzalez and H. B. Schlegel, *J. Phys. Chem.*, 1990, **94**, 5523–5527.
28 J. A. Pople, M. Head-Gordon and K. Raghavachari, *J. Chem. Phys.*, 1987, **87**, 5968–5975.
29 A. P. Scott and L. Radom, *J. Phys. Chem.*, 1996, **100**, 16502–16513.
30 T. J. Lee and P. R. Taylor, *Int. J. Quantum Chem., Quantum Chem. Symp.*, 1989, **23**, 199–207.
31 J. C. Rienstra-Kiracofe, W. D. Allen and H. F. Schaefer III, *J. Phys. Chem. A*, 2000, **104**, 9823–9840.
32 P. J. Robinson and K. A. Holbrook, *Unimolecular Reactions*, John Wiley & Sons, 1972.
33 D. R. Glowacki, C. H. Liang, C. Morley, M. J. Pilling and S. H. Robertson, *J. Phys. Chem. A*, 2012, **116**, 9545–9560.
34 M. B. Blanco, I. Bejan, I. Barnes, P. Wiesen and M. A. Teruel, *Environ. Sci. Pollut. Res.*, 2009, **16**, 641–648.
35 D. Grosjean and E. L. Williams, *Atmos. Environ., Part A*, 1992, **26**, 1395–1405.
36 W. H. Wang, M. J. Ezell, A. A. Ezell, G. Soskin and B. J. Finlayson, *Phys. Chem. Chem. Phys.*, 2002, **4**, 1824–1831.
37 M. Ullerstam, E. Ljungström and S. Langer, *Phys. Chem. Chem. Phys.*, 2001, **3**, 986–992.
38 C. E. Canosa-Mas, E. S. N. Cotter, J. Duffy, K. C. Thompson and R. P. Wayne, *Phys. Chem. Chem. Phys.*, 2001, **3**, 3075–3084.
39 C. E. Canosa-Mas, H. R. Hutton-Squire, M. D. King, D. J. Stewart, K. C. Thompson and R. P. Wayne, *J. Atmos. Chem.*, 1999, **34**, 163–170.
40 B. J. Finlayson-Pitts, C. J. Keoshian, B. Buehler and A. A. Ezell, *Int. J. Chem. Kinet.*, 1999, **31**, 491–499.